Advanced Powder Technol., Vol. 17, No. 6, pp. 641–662 (2006)

Also available online - www.brill.nl/apt

Original paper

A hybrid numerical model for predicting segregation during core flow discharge

NICHOLAS CHRISTAKIS [1,*], PIERRE CHAPELLE [2], NADEZHDA STRUSEVICH [3], IAN BRIDLE [4], JOHN BAXTER [5], MAYUR K. PATEL [3], MARK CROSS [6], UGUR TÜZÜN [5], ALAN R. REED [4] and MICHAEL S. A. BRADLEY [4]

[1] *Department of Applied Mathematics, University of Crete, Heraklion 71409, Greece*
[2] *Laboratoire de Science et Génie des Matériaux et de Métallurgie, Ecole de Mines, Nancy 54042, France*
[3] *School of Computing and Mathematical Sciences, University of Greenwich, London SE10 9LS, UK*
[4] *The Wolfson Centre for Bulk Solids Handling Technology, University of Greenwich, London SE18 6PF, UK*
[5] *Chemical and Process Engineering, School of Engineering, University of Surrey, Guildford GU2 7XH, UK*
[6] *Chemical Engineering, School of Engineering, University of Swansea, Swansea SA2 8PP, UK*

Received 22 December 2005; accepted 24 March 2006

Abstract—A continuum numerical model is presented that parameterizes the interactions between particles at the microscopic level and predicts the development of moving stagnant zone boundaries during core flow discharge of granular material. The model is then employed for the prediction of segregation of multi-component granular mixtures during discharge from core flow hoppers and its capability to accurately simulate the behavior of the granular mixture is demonstrated through comparisons with experimental data.

Keywords: Granular material; core flow; segregation; continuum modeling; micro-physical parametrizations.

1. INTRODUCTION

The flow of granular material is a very important transport process, occurring in a number of applications in the process engineering industry. In recent years, significant effort has been put into the modeling of granular material flow, and a number of analytical and numerical models have been developed to describe it (e.g. Refs [1–10]). Granular dynamics and micro-physical models have been successful

*To whom correspondence should be addressed. E-mail : nchristakis@tem.uoc.gr

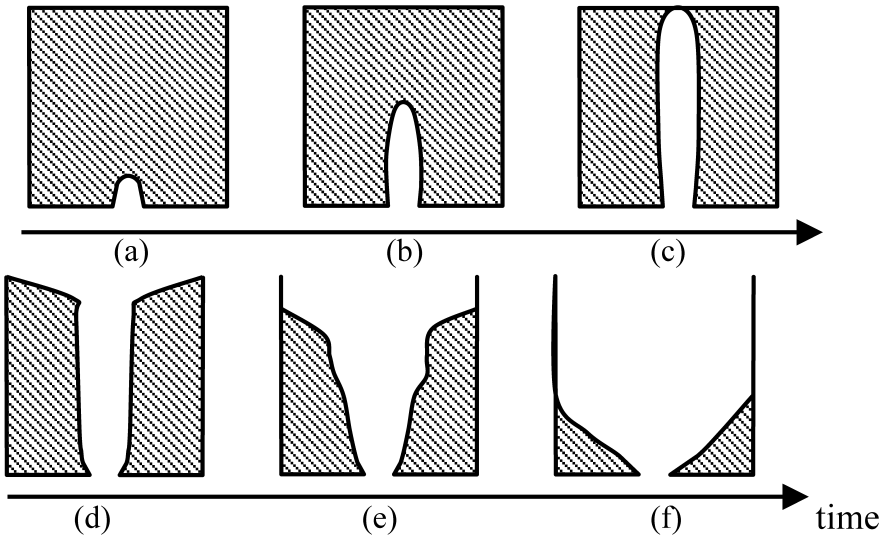

Figure 1. Development with time of the stagnant zone boundaries during core flow discharge from a flat-bottomed hopper. The dashed areas represent stagnant zones where material does not flow.

in describing the flow of granular material by accounting for the interactions between particles at the microscopic level (see, e.g. Refs [6, 10]). However, these models can only be applied to relatively small numbers of discrete particles, due to the complexity of the simulated physical processes. Thus, such models would not be suitable for the direct simulation of large-scale processes which involve granular material, due to the considerable amount of computing time and memory required to simulate processes that involve a very large number (i.e. billions) of discrete particles.

Models based on a continuum mechanics approach are the most suitable for simulating large-scale granular flow processes. Particular mention should be made of models employing viscoplastic flow rules (see, e.g. Refs [7–9]). These models have been partially successful in capturing some of the main characteristics of the flow. However, they lack essential information on particle–particle interactions and material parameters at the microscopic level, hence they are incomplete and cannot be employed to simulate granular flow processes which might lead to phenomena such as particle size segregation.

Two distinct types of flow may be identified during granular material discharge: mass flow, where all material regions in the domain are in motion, and core flow, where there is a moving material channel above the orifice of the emptying hopper and stagnant material zones further away from the flowing channel. The development of the stagnant zone boundaries, based on experimental observations (e.g. Ref. [11]), can be schematically seen in Fig. 1, with the dashed area representing the stagnant zones where the material does not flow. During the initial stage (which only lasts a very short time compared to the latter stages of

discharge), the flowing zone is a narrow channel above the orifice, which grows very rapidly in length (Fig. 1a–c). When the flowing zone reaches the top surface, its sides steepen until the material angle of repose is reached (an intrinsic material property, expressing the internal particle–particle friction, e.g. Ref. [11]) and begins to descend slowly, with material rolling down the interface into the flowing channel and the flowing zone becoming gradually wider (Fig. 1d and f). Finally, when the top surface of the stagnant zone boundary (which is at the angle of repose) intersects the plane of the orifice (Fig. 1f), the discharge stops and no more material exits from the hopper. It can be established *a priori* whether a hopper goes into core flow or mass flow through semi-empirical engineering criteria, which take into account the hopper geometry and material properties [11].

Recently, a continuum numerical model was presented that employed micro-physical parameterizations derived in a granular dynamics framework, in order to model particle size segregation of granular mixtures during mass flow discharge from hoppers. Very good agreement was established between numerical predictions and available experimental data [12]. The modeling of granular material discharge in core flow mode is, however, more complicated because of the existence of stagnant zones. Unfortunately, no reliable method exists for predicting the shape of the stagnant zone boundaries, although this has been a subject of intensive research for the past 40 years.

Jenike [13, 14] pioneered a method that is based on concepts of plasticity theory and employs a failure criterion in order to predict the shape of stagnant zone boundaries. However, it was found [15] that the flowing zones predicted by Jenike's radial velocity field are narrower than the ones observed experimentally. The above analysis, of course, considers the granular material as a plastic continuum, whilst the discrete nature of the granular material was reflected in the kinematic model [16–18]. The kinematic model has its foundation in statistical mechanics and assumes that as the particles of one layer move, the vacated space is filled by particles of the layer above. This model postulates a linear relationship between the horizontal velocity and the horizontal gradient of the vertical velocity. This relationship depends only on one empirical material parameter, called the kinematic constant, which has dimensions of length. The kinematic model was applied with some success to centric flat-bottomed hopper discharges and was recently applied to eccentric discharges of flat-bottomed vessels [19], where the kinematic constant was correlated to the height of the stagnant zone. However, since the solutions predicted by the kinematic model for the stagnant zone boundaries are parabolic in nature and, hence, cannot have discontinuous solutions, the kinematic model cannot be employed under unsteady-state conditions. For this reason, a modified kinematic model was proposed by Nedderman [20], which accounts for the changing shape of the flowing zone and the dilation occurring at the initiation of the flow. Here, good agreement was established between the model predictions and experimental measurements from flat-bottomed hoppers reported in Watson [21].

In the present paper, the modified kinematic model is implemented into a continuum mechanics framework and extended to enable the modeling of core flow of multi-component granular mixtures in hoppers that incorporate conical sections. The capability of the model to realistically represent core flow processes and predict particle segregation during discharge is then demonstrated in a series of simulations, which involve centric discharges of multi-component mixtures and for which corresponding experimental data were available.

2. THE CONTINUUM FRAMEWORK

In this section, we summarize the governing equations of the continuum model. A more detailed discussion on the many continuum models described in the literature, and the consistency and effectiveness of the various assumptions and simplifications employed to develop the current model are given in Ref. [12]. The continuum framework is employed to solve the conservation equations for mass, momentum and energy for an N-species granular mixture. The full set of equations was solved using PHYSICA, a three-dimensional, unstructured, finite-volume modular suite of software, developed at the University of Greenwich [22]. For reasons of simplification, only three momentum equations for the bulk (the sum of all N-species and air in a control volume) were solved and no energy equations were solved.

2.1. The species transport equation

The calculation of each of the individual material components f_i (fractional volume of component i in control volume, $0.0 \leqslant f_i < 1.0$ and total material fraction $= \sum f_i \leqslant$ maximum packing fraction < 1.0) is performed through the solution of a transport equation, which in the absence of sinks or sources is written as:

$$\frac{\partial f_i}{\partial t} + \nabla \cdot (f_i \vec{u}_\mathrm{b} + \vec{J}_{\mathrm{seg}\ i}) = 0, \tag{1}$$

where $\vec{u}_\mathrm{b}$ is the bulk velocity vector and $\vec{J}_{\mathrm{seg}\ i}$ is the segregation 'drift' flux, which describes the motion of each individual species relative to each other. Segregation might occur due to three mechanisms: (i) 'shear-induced segregation' due to gradients of bulk strain rate (mostly for the coarser components of the mixture), (ii) 'diffusion' due to concentration gradients (mostly for the finer components of the mixture — the response mechanism to shear-induced segregation), and (iii) 'gravity-driven spontaneous percolation', a mechanism which tends to drive the fine components of a granular mixture in the direction of gravity through any existing void spaces in the coarse phase matrix and does not depend on any thermodynamic property of the mixture.

Functional forms for the three segregation fluxes, involving characteristic transport coefficients of each mechanism, have been extracted using principles of kinetic theory. The procedure for calculating the transport coefficients consists of perform-

ing simulations using the discrete element method (DEM) on a suitably limited number of particles for a selected set of process conditions within the 'envelope' of conditions in the process of interest. The transport coefficients are calculated from the data of each simulation by integration of the relevant time-correlation function [23] and are then applied in the continuum framework to provide predictions of bulk material behavior. A more detailed description on the functional forms of the three individual segregation fluxes and the calculation method of the transport coefficients are given in Refs [12, 23].

2.2. The momentum equation

The momentum conservation equation for the bulk may be written as:

$$\rho_{\mathrm{b}}\frac{\partial \vec{u}_{\mathrm{b}}}{\partial t} + \nabla\cdot(\rho_{\mathrm{b}}\vec{u}_{\mathrm{b}}\vec{u}_{\mathrm{b}}) = -\vec{\nabla}\, p + \nabla\cdot(\mu_{\mathrm{b}}\vec{\nabla}\vec{u}_{\mathrm{b}}) + \vec{S}, \tag{2}$$

where p is the pressure and $\vec{S}$ is a source term (i.e. gravity, etc.). The parameters ρ_{b} and μ_{b} (introduced in Ref. [12]) are the bulk material density and pseudo-viscosity (equivalent to fluid viscosity), respectively. They are calculated through averaging of the properties of the mixture components, ρ_{gran} and μ_{gran} (solids density and pseudo-viscosity of granular material) and air ρ_{air} and μ_{air} (density and viscosity of air):

$$\rho_{\mathrm{b}} = \sum_i f_i\rho_{\mathrm{gran}} + \left(1 - \sum_i f_i\right)\rho_{\mathrm{air}}, \tag{2a}$$

$$\mu_{\mathrm{b}} = \sum_i f_i\mu_{\mathrm{gran}} + \left(1 - \sum_i f_i\right)\mu_{\mathrm{air}}. \tag{2b}$$

The role of the pseudo-viscosity in the momentum equation is crucial in dictating the evolution of the flow. The higher its value, the more 'viscous' the granular material becomes, causing the deceleration of the flow. As becomes obvious, if different regions of the material domain experienced different 'viscous' forces at different times, this would affect the material flowability, causing it to flow more slowly in the regions where the pseudo-viscosity is higher (thus the shear forces acting like friction forces to the flow). In this way, if the evolution of the stagnant zone boundaries during core flow could be determined, the granular material pseudo-viscosity could be set accordingly in stagnant regions, so that negligible flow occurs in those regions on the timescale of the simulation. For this reason, the modified kinematic model [20] was employed, in order to determine the temporal evolution of the stagnant zone boundaries.

2.3. Numerical method

The momentum conservation equation for the granular mixture was solved using a SIMPLE-based algorithm and a conjugate gradient iterative solver. A total variation

diminishing (TVD) based scheme [scalar equation algorithm (SEA)] proposed by Pericleous *et al*. [24] was used for the discretization of the transport equation for each individual material component. As will be discussed in Section 4, for reasons of numerical stability μ_{gran} was not allowed to vary unbounded, in order to avoid the generation of spurious oscillations of pressure and velocity values during the iterative solution procedure. A more detailed description of the numerical techniques and algorithms can be found in Ref. [12].

3. PARAMETERIZATION OF THE EVOLUTION OF THE STAGNANT ZONE BOUNDARY

The analysis of Nedderman [20] for predicting the development with time of the stagnant zone boundary during discharge was conducted for a flat-bottomed cylindrical hopper. However, as was shown by experimental observations in Tüzün [25], the shape and size of the stagnant zones during core flow discharge do not change if a hopper incorporates a conical section, provided that the vertical height and the size of the outlet of the two hoppers (flat-bottomed and hopper with conical section) remain the same. Hence, the analysis conducted on a flat-bottomed hopper can easily be extended and applied to a hopper with a conical section. Nevertheless, appropriate modifications should be made to account for the hopper conical section, when the correction procedure of Nedderman [20] is applied for the accurate representation of the shape of the stagnant zone boundaries at the latter stages of the discharge.

Nedderman's analysis is based on a modification of the Nedderman and Tüzün kinematic model [17], taking into account the dilation that occurs at the onset of the flow. In spite of its limitations (e.g. axisymmetric hopper), Nedderman's model has been accepted as a reliable method for predicting the size and shape of the stagnant region under unsteady conditions. DEM simulations presented by Masson and Martinez seem in particular to support Nedderman's model [26]. In contrast to the relative success of the kinematic approach and the DEM, it should be mentioned that continuum analyses, despite extensive research efforts, still fail to capture the shape of the stagnant zone during core flow discharge.

As already discussed, the Nedderman and Tüzün kinematic model postulates a linear relationship between the horizontal velocity and the horizontal gradient of the vertical velocity. This relationship depends only on one empirical material parameter B, called the kinematic constant, which has dimensions of length. Exploiting the similarity of the kinematic model equation to diffusion equations (see, e.g. Ref. [27]), an approximate solution of the velocity distribution is first determined by considering the discharge from a point sink in a semi-infinite medium. By expressing the velocity in terms of the stream function and integrating the relation obtained along a streamline, the time taken for a particle originally at any location in the bin to reach the outlet can then be calculated. From this and by making allowance for the voidage changes that occur at the initiation of the motion,

the following equation of the stagnant zone boundary at time T is obtained:

$$T = \frac{2B\pi z^2 \Delta\rho}{Q\rho_{\mathrm{fl}}} \exp\left(\frac{r^2}{4Bz}\right), \tag{3}$$

where r and z are cylindrical coordinates expressing radial and vertical distances, respectively, of a particle from the hopper outlet (measured from the outlet centre), Q is the discharge volumetric flow rate, $\Delta\rho$ is the change of materials bulk density which accompanies the initiation of the motion (i.e. the difference between the bulk densities of stagnant and flowing material regions), ρ_{fl} is the bulk density of the flowing material region, and B is the kinematic constant whose value is often of the order of a particle diameter [18].

It was found, via inspection and comparisons with experiments specifically conducted for the present work, that the best agreement was reached when the values of B were between the particle diameter and 2.2 times the particle diameter. In the current work, the lower value was preferred, since it was consistent with Nedderman's considerations for B [20] and gave the better fit (both qualitative and quantitative) to available experimental data, as will be demonstrated during the presentation of results. Since all previous analysis based on the kinematic model (e.g. Refs [16–20]) concentrated on mono-sized material, while the present work deals with multi-component mixtures of varying sizes, a number average of all particle diameters was chosen as the particle diameter in the equation for B. Following Refs [15, 20], the ratio $\Delta\rho/\rho_{\mathrm{fl}}$ was taken as 0.1 and was kept constant for all performed simulations. The discharge volumetric flow rate Q through a circular outlet under free-fall conditions may be obtained through the following semi-empirical correlation [20]: $0.58g^{1/2}d_{\mathrm{out}}^{5/2}$, where d_{out} is the outlet diameter and g is the gravitational constant. This equation assumes that particle diameter is much smaller than the orifice diameter. If the hopper is not simply flat-bottomed, but incorporates a conical section of hopper half-angle a, the equation for the flow rate becomes (see, e.g. Ref. [11]): $0.58g^{1/2}d_{\mathrm{out}}^{5/2}(\tan a)^{-0.35}$. However, in most industrial applications the discharge of material from hoppers is performed using a controlled flow rate, by pulling material from the outlet at a fixed velocity.

According to (3), the boundaries between the flowing and stationary solids are paraboloids of revolution. Since (3) was derived based on the assumption of discharge from a semi-infinite medium, it can only apply to intermediate heights. Later stages of the discharge, where the flowing zone reaches the upper free surface or the side walls, require a specific treatment. In those stages, the equation of the stagnant zone boundary is modified near the upper free surface and the walls as follows, according to experimental observations. After the boundary intersects the solids upper free surface and then starts expanding laterally, the upper sides of the flow channel boundary are defined as a conical surface at the angle of repose of the material (as illustrated in Fig. 1d and f). The height h of the outer edge of the top free surface below the original level is obtained from a balance on the volume of the material discharged (by assuming that the flowing channel is always

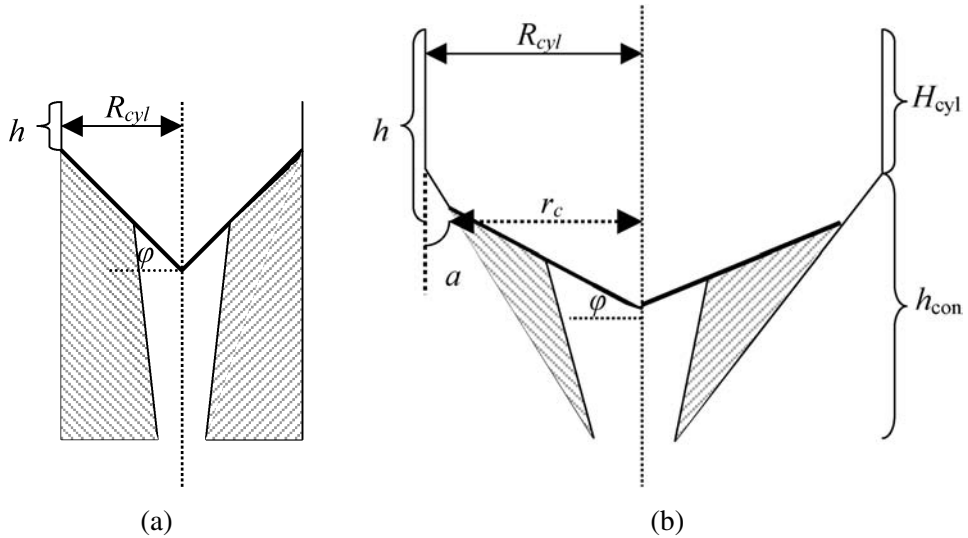

Figure 2. Stagnant zone boundary (dashed area indicating stagnant zones) and air–material interface (thick line) at angle of repose during later stages of core flow discharge: (a) flat-bottomed cylindrical hopper and (b) cylindrical hopper incorporating a conical section. Note that the flowing channel around the central axis of the hopper is maintained filled with material.

maintained filled and that the top air–material interface between wall and outlet axis is always maintained at the angle of repose, see Fig. 2a). Hence, as Nedderman [20] postulates, for a flat-bottomed cylindrical hopper:

$$QT = \pi R_{\mathrm{cyl}}^2 h + \pi/3 R_{\mathrm{cyl}}^3 \tan\phi, \tag{4}$$

where R_{cyl} is the hopper radius and ϕ is the material angle of repose.

In the case of a hopper including a conical section, (4) needs to be modified within the conical section to account for the different volume balance. In this case, the volume of the discharged material consists of three volumes (see Fig. 2b): the volume of the cylindrical section, the volume of the cone of radii R_{cyl} and r_{c} and height $(h - H_{\mathrm{cyl}})$ and the volume of the right circular cone of radius r_{c} and height $r_{\mathrm{c}} \tan\phi$. The modified volume balance for points within the conical section may then be written as:

$$QT = \pi R_{\mathrm{cyl}}^2 H_{\mathrm{cyl}} + \pi \frac{h - H_{\mathrm{cyl}}}{3}\left(R_{\mathrm{cyl}}^2 + R_{\mathrm{cyl}} r_{\mathrm{c}} + r_{\mathrm{c}}^2\right) + \pi/3 r_{\mathrm{c}}^3 \tan\phi, \tag{5}$$

where radius r_{c} can be easily related to height h through the equation $r_{\mathrm{c}} = R_{\mathrm{cyl}} - (h - H_{\mathrm{cyl}}) \tan a$.

In this way, the parabolic curves of (3) may be corrected for the later stages of the discharge once the top surface has formed its conical shape. The discharge associated with the changes in density has been omitted, since it would introduce further uncertainties during the early stages of discharge [20].

The position of the final stagnant zone may be determined by following the straight line at the material angle of repose, which intersects the plane of the hopper outlet (see Fig. 1f). Material below that line is retained indefinitely in the hopper. For the case of a flat-bottomed hopper, a stagnant zone will always be present at the end of a core flow discharge, while for a hopper with a conical section, there will be material left only if $(\pi/2 - a) < \varphi$ or if $(R_{\text{cyl}} - r_{\text{out}}) > h_{\text{con}} \tan a$, where h_{con} is the vertical height of the conical section, r_{out} is the radius of the outlet and a is the hopper half-angle (i.e. for the case of a circular insert at the bottom of the hopper, in order to decrease the diameter of the outlet).

4. SOLUTION PROCEDURE

Through (3) and the applied corrections through (4) and (5) for the later stages of discharge, the evolution of the flow–no flow boundaries may be determined at the onset of a simulation of core flow discharge, since its calculation did not require any of the PHYSICA solved parameters (i.e. velocities, pressures, material fractions). Hence, the critical times T for all material regions in the domain may be determined, which correspond to the time intervals after which these regions are allowed to flow. As already discussed, the flow may be controlled via the granular dynamic pseudo-viscosity term μ_{gran} of (2b). Accordingly, during the solution of the momentum equation, appropriate values for μ_{gran} were employed, which either stopped the material from flowing or allowed flow. A value for μ_{gran}, obtained through trial and error, which leads to a negligible flow of the material on the timescale of the simulation, was $\mu_{\text{gran max}} = 10^6\ \text{m}^{-1}\,\text{kg}\,\text{s}^{-1}$. This value was employed in the stagnant material zones in order to impose a very slow deformation rate to the material (i.e. stop the material from flowing). It was also set as the initial granular pseudo-viscosity at the start of a simulation. When simulation time reached the critical time T for a material region, a different pseudo-viscosity $\mu_{\text{gran fl}}$, which would allow flow, had to be employed.

In the flowing regions, a dynamic pseudo-viscosity $\mu_{\text{gran fl}}$ was derived, based on the Drucker–Prager yield criterion. Viscoplastic constitutive models have proved to give a realistic estimation of the behavior of granular materials [28]. Among them, viscoplastic models based on the Drucker–Prager yield function have been widely used to successfully describe granular flows in silos (see, e.g. Ref. [29]). Recently, such a model which utilizes the Drucker–Prager yield function and simulates the segregation behavior of granular mixtures during silo charging has been developed and validated [30]. This viscoplastic model is employed in the present work to represent the pseudo-viscosity $\mu_{\text{gran fl}}$ in the flowing regions as a non-linear function of pressure, the material angle of repose and the bulk velocity gradients. An upper bounding value for $\mu_{\text{gran fl}}$, equal to $\mu_{\text{gran max}}$, was employed so that the material pseudo-viscosity would not exceed its maximum no-flow value.

In order to avoid numerical instabilities at the transition between flowing and non-flowing domains due to high velocity gradients, a thin transition region between

the flowing and non-flowing parts was considered. In this transition region, the viscosity was assumed to vary linearly between the upper bound value of the viscosity $\mu_{\text{gran max}}$ and the average value of the viscosity within the flowing region.

During a time-step, once convergence was achieved in the calculation of pressures and velocities, the converged velocity values were employed for the solution of the species transport equations in order to determine the movement of the individual species in the bulk and the corresponding levels of size segregation.

5. DETERMINATION OF INITIAL CONDITIONS

Special consideration was given to initial conditions, in order to correctly represent the initial state of the granular mixture before the discharge. The initial stress state of the material resting in the hopper may be obtained using balance of forces, and, thus, connecting normal stresses to material properties, hopper properties and dimensions, and gravity (see, e.g. Ref. [11]). An example of such calculation for a mono-sized material resting in a conical hopper is given in Fig. 3, where mean normal stress contours and major–minor stress vectors are presented. Note that mean normal stress does not vary linearly with height and that there is a switch in the major–minor stress vectors, following the switch in geometry for the hopper

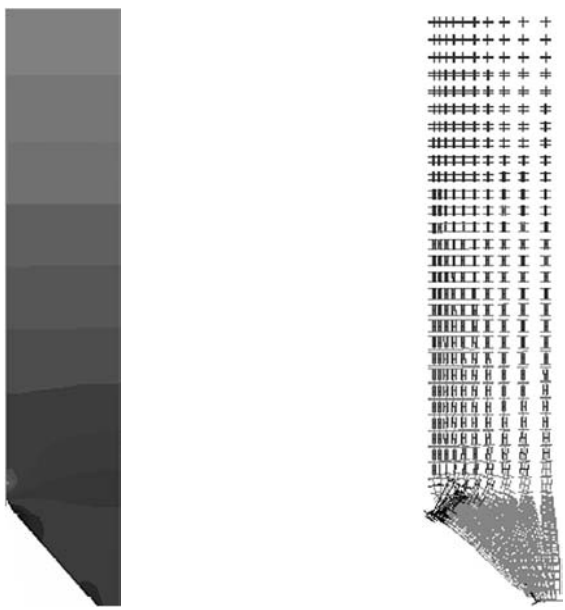

Figure 3. (a) Initial mean normal stress distribution and (b) major–minor stress vectors for a mono-sized granular material resting in a conical hopper. The colour scale represents stress intensity in a computational cell (i.e. light colours indicate lower stress state, darker colours indicate higher stress state).

from cylinder to cone. Since the studied discharges were centric (i.e. the outlet was located around the central axis of symmetry of the hopper), for reasons of simplicity and due to the observed symmetry of the flow around the hopper central axis, a semi-three-dimensional geometry, of a hopper slice of 5° angle around the central axis of symmetry, was chosen as the most appropriate geometry for the performed simulations. The consistency of this assumption for centric granular material discharges was demonstrated in Ref. [12].

The initial fill state of the mixtures was obtained directly through the use of an experimental device called the segregation tester, which provides details of the material composition radial distribution during the filling process of a hopper and the resulting radial segregation patterns [31]. The segregation tester consists of a rotating transparent mixer and a parallelepiped section underneath the mixer, which is adjusted to an inclination in order to represent the material angle of repose (Fig. 4). The parallelepiped section is divided into five compartments, which can be separated after the end of the filling process by inserting vertical steel plates between them, so that material may be analysed from each compartment separately.

The corresponding radial distribution of the mixture at fill within the hopper is obtained through re-scaling of the mixture compositions obtained in the segregation tester. For hopper centric charge, the mixture composition from the most elevated compartment of the parallelepiped section of the segregation tester corresponds to the mixture composition in regions around the hopper central axis, while the composition from the least elevated part of the parallelepiped section corresponds to the composition in regions closer to the hopper walls. It is expected that the coarser particles, during the filling process, will roll along the interface and will

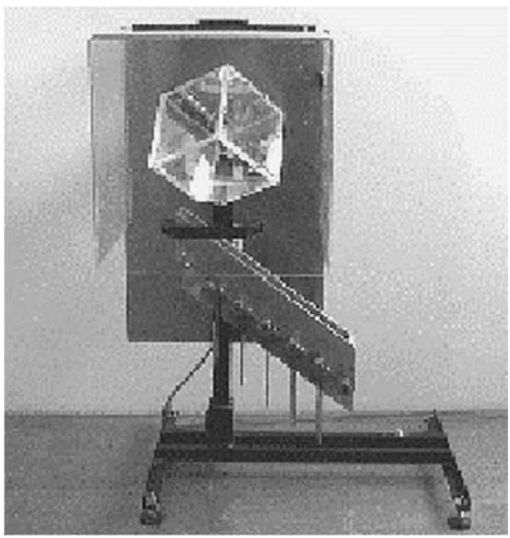

Figure 4. Segregation tester. Experimental device to assess material radial segregation during the filling operation of a silo.

concentrate further away from the axis of filling, while the finer particles are expected to concentrate around the axis of filling [31]. The segregation tester has been shown to accurately predict the radial segregation patterns at fill of small to medium height (less than about 1 m in height) hoppers, for relatively moderate size ratio mixtures, where the components are not very different in size and, hence, gravity-driven percolation does not constitute a problem [31].

6. NUMERICAL SIMULATIONS AND TESTING OF THE MODEL

The numerical model was first tested for consistency with data presented in Nedderman [20], and was then employed to simulate core flow discharges of a binary granular mixture from a flat-bottomed cylindrical hopper and of a ternary granular mixture from a hopper which incorporates a conical section, for which experimental data were available. The hopper geometries, material properties and operating parameters used in the three different simulations performed are presented in Table 1. As already noted, a semi-three-simensional geometry of a hopper slice of 5° angle around the central axis of symmetry was chosen as the most appropriate geometry for the performed simulations. The computational meshes used in the three different simulations are shown in Fig. 5. The number of mesh elements and the maximum time steps used for each simulation are given in Table 1.

Table 1.
Parameters used in the simulations performed

Parameters	Consistency test (Section 6.1)	Flat-bottomed hopper (Section 6.2)	Hopper with conical section (Section 6.3)
Cylindrical section height (m)	0.94	0.77	0.75
Cylindrical section diameter (m)	0.65	0.55	0.80
Conical section height (m)	0	0	0.65
Outlet diameter (m)	0.065	0.075	0.075
Material	polypropylene	lytag	lytag
Angle of repose (°)	34	32	32
Solids density (kg/m^3)	900	825	825
Maximum packing fraction	0.66	0.66	0.66
Size distribution			
no. of size fractions	1	2	3
particle diameter (mm)	5	5.2/2.6	7.8/5.5/2.6
weight fraction (%)	100	40/60	33.3/33.3/33.3
Volumetric discharge rate (m^3/s)	0.98×10^{-3}	2.8×10^{-3}	1.4×10^{-3}
No. of elements in the computational mesh (r, z)	14×40	14×20	18×70
Maximum time steps (s)	10^{-3}	10^{-3}	10^{-3}

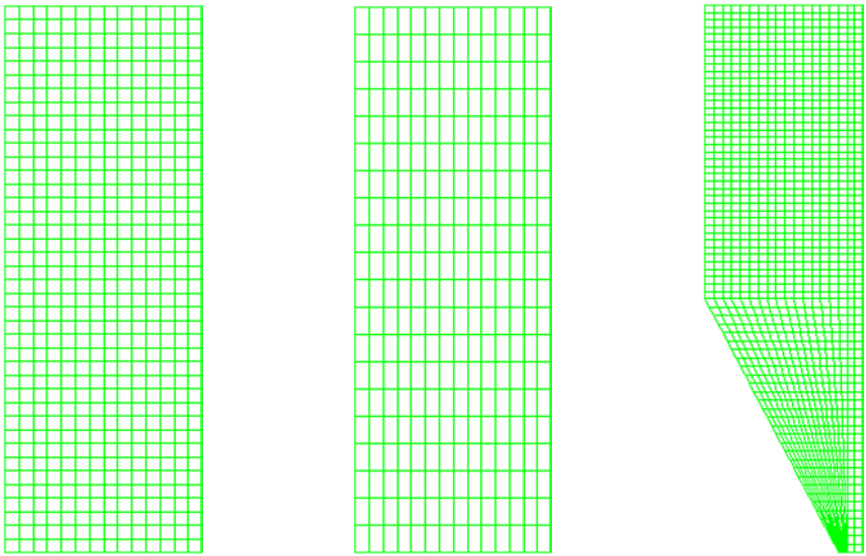

Figure 5. Mesh used in the calculations: (a) consistency test (Section 6.1), (b) flat-bottomed hopper (Section 6.2) and (c) hopper with conical section (Section 6.3). This figure is published in color on http://www.ingenta.com

6.1. Consistency test

To test the consistency of the proposed model, a simulation was performed for the conditions corresponding to the experimental work of Watson [21] and chosen by Nedderman to apply his modified kinematic model [20]. Watson [21] considered the core flow discharge of a mono-sized material from a cylindrical flat-bottomed hopper. The hopper was totally filled and the top free surface of the material was flat. Since this study was performed for a mono-sized material, the segregation coefficients (i.e. coefficients for shear-induced segregation, diffusion and gravity-driven percolation) required in (1) were taken as 0.

The temporal evolution of the stagnant zone boundaries predicted by PHYSICA is presented in Fig. 6a. Reasonable agreement is found to exist between the predictions of Nedderman (Fig. 4 in Ref. [20]) and those of the present model for the temporal evolution of the stagnant zone boundary. The flow boundary was seen to propagate rapidly to the top of the hopper (in less than 23 s), and then to widen and descend very slowly, with the top surface of the material inclined at the material angle of repose. The total discharge time calculated by Nedderman (249.8 s) closely agreed with the discharge time of 250 s predicted by PHYSICA. In Fig. 6b, a comparison is presented between PHYSICA and Nedderman calculations for the width of the flowing zone at half-height (47 cm) of the hopper. The results were in reasonable agreement, their relative difference always being less than 8%. The flowing zone expanded rapidly during the early stages of the discharge and thereafter at a much

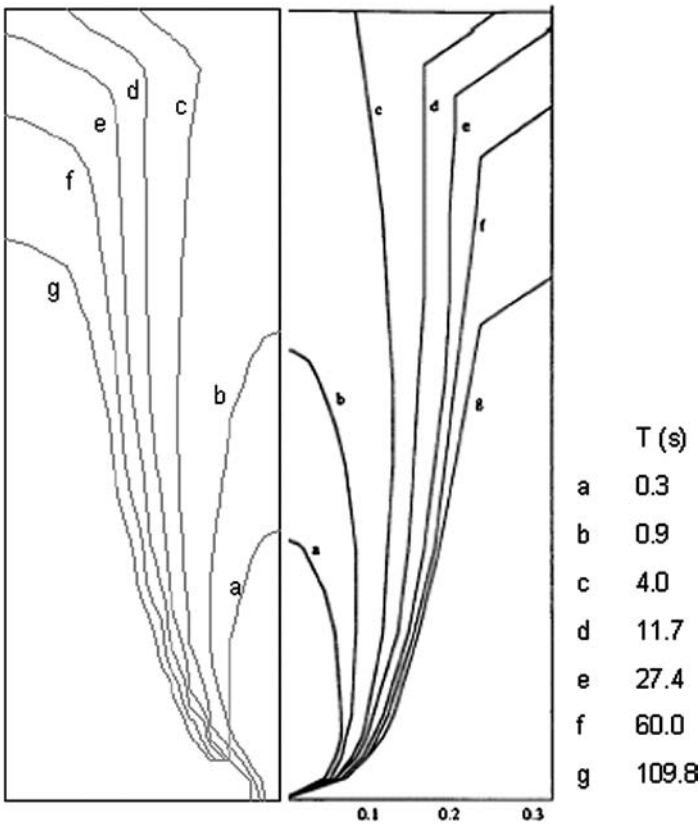

(a)

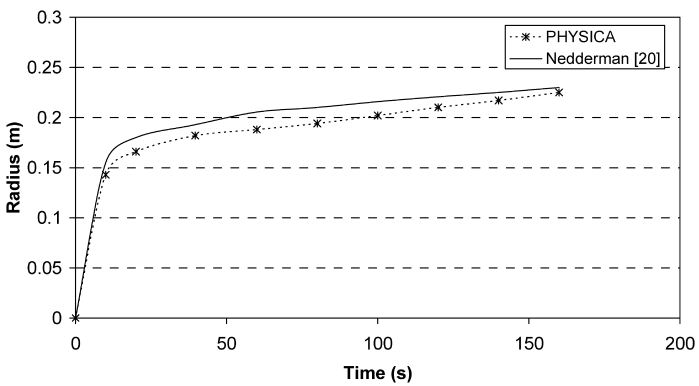

(b)

Figure 6. Comparison of the temporal evolutions of (a) the position of the stagnant zone boundary and (b) the width of the stagnant zone boundary at half height predicted by the present model with the results by Nedderman [20]. Stagnant zone boundaries on the left-hand side are the present calculations and those on the right-hand side are the results by Nedderman (which are taken from Ref. [20]).

slower rate. The plot does no go beyond $t = 160$ s, as the top surface of the stagnant zone was predicted in both instances to be located below the half-height level after that time.

6.2. Discharge of a binary mixture from a flat-bottomed hopper

In this section, the simulation of core flow discharge and segregation of a binary granular mixture from a flat-bottomed cylindrical hopper, for which experimental data were available, is presented. The flat-bottomed hopper was centrally filled from the top using a static blender (validated by Salter [31]). This methodology of filling ensured that a fully blended mix entered the core flow hopper. The hopper was filled with material to its full height (i.e. 77 cm) and it was ensured that the material interface at the top was flat. On emptying of the hopper, a sampling tray was passed underneath the outlet through the full stream of material at set time intervals, enabling representative samples to be obtained for the total duration of the emptying process (approximately 60 s). To investigate the amount of segregation attained in this work, particle size distributions of the material samples were measured. Particle size analysis was undertaken according to the British Standard procedure for conducting a manual sieve test [32].

For the simulation of the above experiment, the initial fill state of the numerical hopper was obtained via the segregation tester and is given in Fig. 7a. The

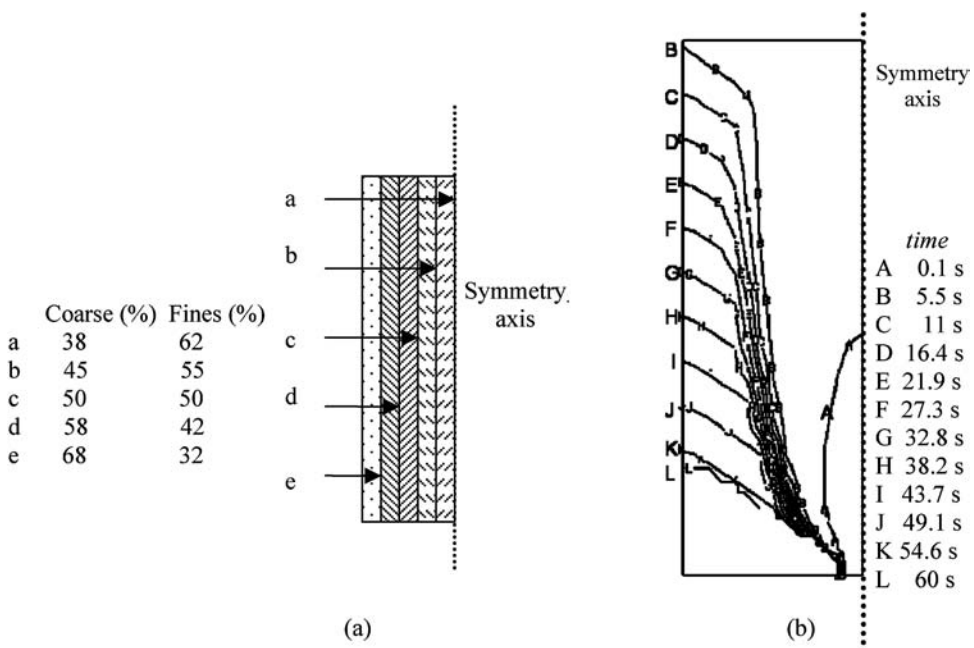

Figure 7. Core flow discharge of lytag 60-40, 2:1 binary mixture from a flat-bottomed hopper. (a) Initial fill state, obtained with the aid of the segregation tester. (b) Temporal evolution of the stagnant zone boundaries.

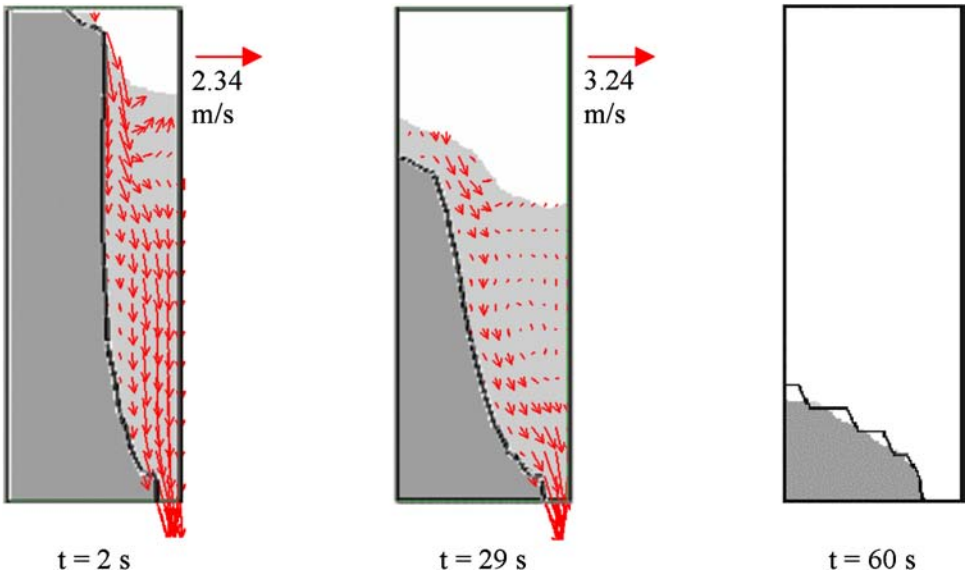

Figure 8. Core flow discharge of lytag 60-40, 2:1 binary mixture from a flat-bottomed hopper. Computed material–air interface, particle velocity and corresponding stagnant zone boundary (solid line) at different times during the discharge. The light (dark) grey area represents the flowing (non-flowing) materials. The vector legend corresponds to the maximum observed velocity at each of the presented times. This figure is published in color on http://www.ingenta.com

segregation transport coefficients were calculated using DEM analysis [23] and were directly imported in the continuum framework. The diffusion coefficients were found to be of the order of 10^{-8} m^2/s for the fines fraction and almost 4 times higher for the coarse fraction. In the case of the shear-induced segregation coefficients, the coefficient for the coarse fraction was found to be of the order of 10^{-6} m^2/s, while the coefficient for the fines fraction was an order of magnitude lower. The percolation mechanism was calculated to be much weaker than the diffusion and shear-induced segregation mechanisms for the particular size ratio considered and a percolation coefficient of the order of 10^{-10} m^2/s was used for the fines fraction in the simulations.

Figure 7b presents the evolution of the stagnant zone boundaries as a function of time. The flowing zone developed very quickly in length and reached the top in less than 5.5 s. Then, it was predicted to widen and descend slowly (maintaining the angle of repose at its top surface), until the position of the final stagnant zone at the material angle of repose was reached (line L in Fig. 7b) between 54.6 and 60 s. This time agreed closely with the experimentally measured discharge time of approximately 60 s. After that stage, no more material was expected to exit the domain. Figure 8 presents the material–air interface, particle velocity and the corresponding stagnant zone boundaries (solid black line in the domain) at various times during the discharge. Note that the interface between material and air was maintained at the angle of repose, with material avalanching into the central channel.

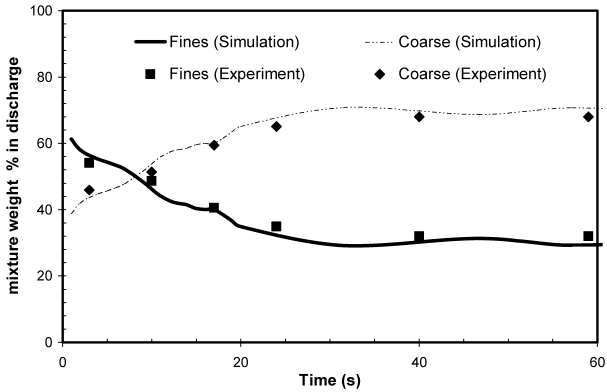

Figure 9. Core flow discharge of lytag 60-40, 2:1 binary mixture from a flat-bottomed hopper. Temporal variation in mixture weight fraction (averaged across outlet).

At the end of the discharge, there was a slight shift between the stagnant zone boundary and the material–air interface, since a relatively coarse grid was used for the computation. As observed in Fig. 8, the distribution of particle velocities during the discharge process is discontinuous. Two principal zones on both sides of the stagnant zone boundary can clearly be distinguished. In the central part of the hopper, the particles are flowing with trajectories converging towards the outlet, whereas in regions close to the walls particles remain at rest. As the flow ceases at the end of the discharge ($t = 60$ s), a region of stationary material is left in the corner of the hopper bottom, in agreement with core flow pattern.

In Fig. 9, the temporal variation in the mixture composition (plotted as mass percentage of the individual fractions), averaged across the outlet, is presented and compared against experimental data collected during the discharge. The amount of finer particles exiting the domain dropped very quickly as a result of the shear-induced segregation/diffusion process, which tends to drive the coarser particles towards regions of high shear (i.e. the flowing zone close to the hopper central axis of symmetry). In general, there seemed to be good agreement between model predictions and experiments, within the experimental uncertainty of 4%. The observed mixture behavior was correctly represented and the particular features of the discharge (i.e. the intersection point between fines and coarse weight fractions) were accurately predicted.

6.3. Discharge of a ternary mixture from a cylindrical hopper incorporating a conical section

This section presents simulation results of the segregation of a ternary granular mixture discharging under core flow mode from a cylindrical hopper including a conical section. The core flow hopper was centrally filled in the same manner as previously discussed in Section 6.2 utilizing a static blender, with a heap forming at the top at the material angle of repose (32°). In this experiment, the mixture

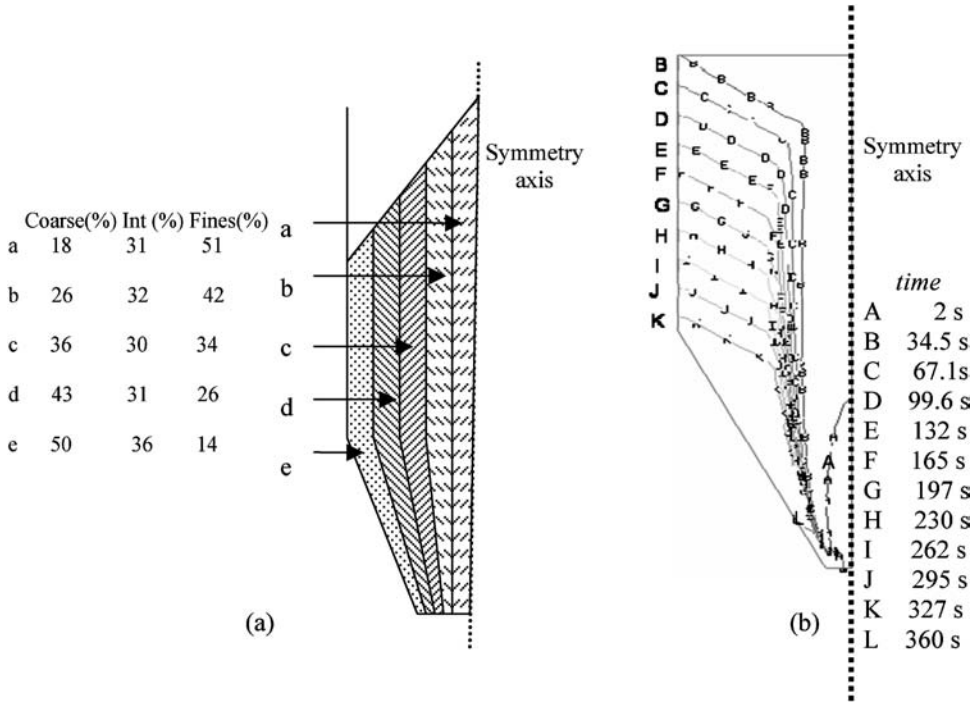

Figure 10. Core flow discharge of lytag 33.3-33.3-33.3, 3:1.9:1 ternary mixture from a cylindrical hopper with a conical section. (a) Initial fill state, obtained with the aid of the segregation tester. (b) Temporal evolution of the stagnant zone boundaries.

discharge was conducted at a controlled volumetric flow rate of 1.4×10^{-3} m^3/s. Samples were obtained on emptying using the same principle as employed for the flat-bottomed vessel in Section 6.2.

The initial segregated fill state was obtained with the aid of the segregation tester and is given in Fig. 10a. DEM analysis was used for the calculation of the segregation transport coefficients [23]. The diffusion coefficients were calculated to be of the order of 10^{-8} m^2/s for the finer fraction and slightly higher (but of the same order of magnitude for the coarser fraction). For the shear-induced segregation, the coefficient for the coarser fraction was found to be of the order of 10^{-6} m^2/s, while the coefficient for the finer fraction was confirmed to be an order of magnitude lower. The coefficients of segregation (shear-induced and diffusion) for the intermediate size class were seen to be much weaker than the respective coefficients of the other fractions, which was confirmed by the radial segregation data at fill provided by the segregation tester. Hence, they were set to values of the order of 10^{-10} m^2/s. It is interesting to note that although the intermediate and finer fractions were almost identical to the coarse and fines fraction examined in Section 6.2, the segregation coefficients for the case of the intermediate fraction (5 mm diameter) were very different to the coefficients of the coarse phase (5.2 mm diameter) of the previous section. This result was anticipated and is in agreement

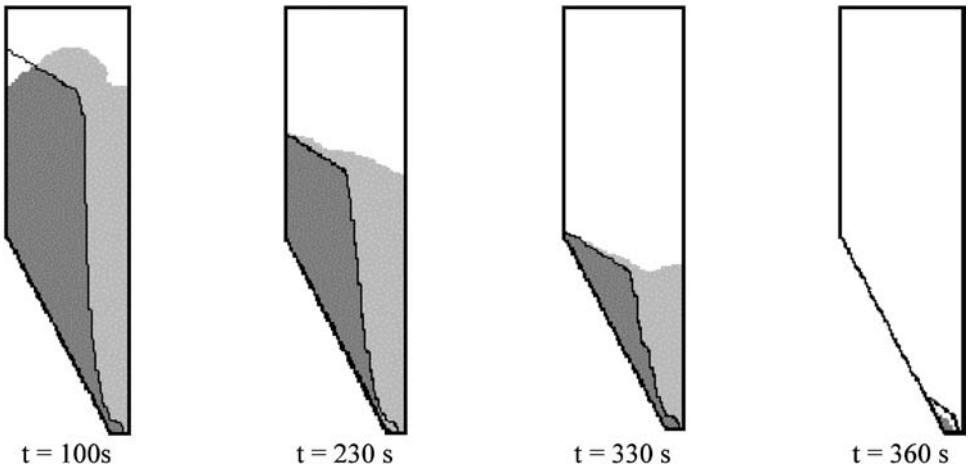

Figure 11. Core flow discharge of lytag 33.3-33.3-33.3, 3:1.9:1 ternary mixture from a cylindrical hopper with a conical section. Computed material–air interface and corresponding stagnant zone boundary (solid line) at different times during the discharge. The light (dark) grey area represents the flowing (non-flowing) materials.

with molecular dynamics theory, where it is argued that the coarsest of all phases in a mixture dictates the segregation patterns (see, e.g. Ref. [23]). Because of the moderate mixture size ratio, gravity-driven percolation in the system was assumed to be very low and a percolation coefficient of the order of 10^{-10} m^2/s was used for the finer fraction in the performed simulations.

Figure 10b presents the temporal evolution of the stagnant zone boundaries. The flowing zone was predicted to develop rapidly in length and reaches the top in less than 35 s. Then, it was seen to widen and descend slowly (maintaining the angle of repose at its top surface), until the final stagnant zone boundary at the material angle of repose was reached (line L in Fig. 10b) at 360 s from the start of the discharge. This time was in reasonable agreement (within 8%) with the experimentally measured discharge time of approximately 330 s. Figure 11 shows the material–air interface and the corresponding stagnant zone boundaries at various times during the discharge. Note that the interface between material and air was maintained at the angle of repose, with material avalanching into the central channel. Like in Fig. 8, the slight shift between the stagnant zone boundary and the material–air interface observed at the end of the discharge is due to the relatively coarse grid used for the computation.

In Fig. 12, the temporal variation in the mixture composition (plotted as mass percentage of the individual fractions), averaged across the outlet, is presented and compared against experimental data collected during the discharge. The model represented correctly the observed mixture behaviour and particular features of the discharge (i.e. the intersection point between fine, intermediate and coarse weight fractions). However, the agreement is only qualitative during the early times of the discharge. At the initial stages of the discharge, the model under-predicted (over-

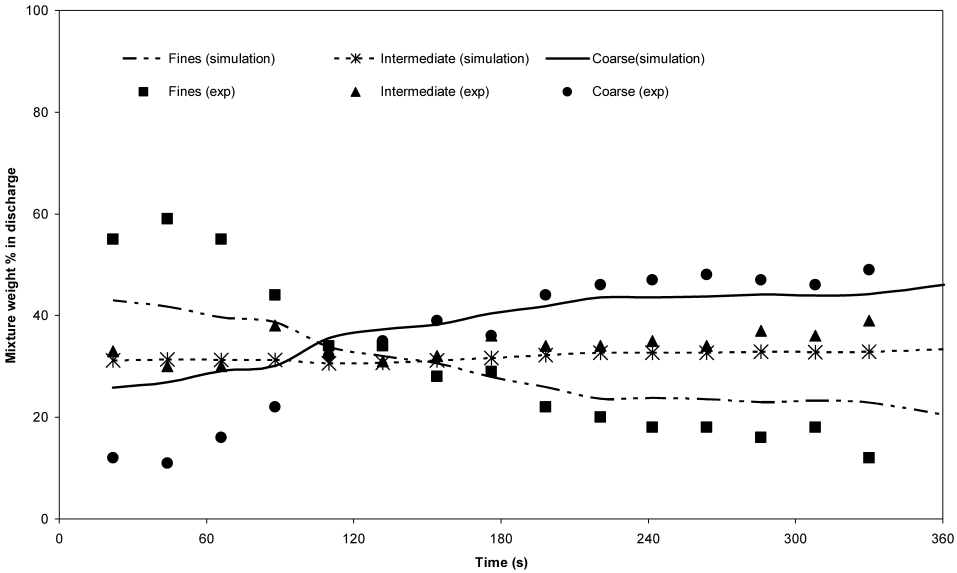

Figure 12. Core flow discharge of lytag 33.3-33.3-33.3, 3:1.9:1 ternary mixture from a cylindrical hopper with a conical section. Temporal variation in mixture weight fraction (averaged across outlet).

predicted) the amount of finer (coarser) material exiting the hopper. This may be attributed to issues in determining the accurate initial material composition resulting from filling. Indeed, the experimental data indicated that some spontaneous percolation occurred during the filling stage (possibly due to non-uniform hopper filling effects), which are not accounted for in the present simulation. As was already mentioned in Section 5, the segregation tester gives a fairly accurate profile of the initial fill state for hoppers less than 1 m in height, but for taller hoppers, even for the moderate size ratio mixture employed, random percolation might not be avoided and the output of the segregation tester should be treated with more caution.

Despite these limitations, the presented numerical model has demonstrated its capability to accurately represent the behavior of granular material during core flow discharges and, using micro-mechanical parametrizations, to predict the segregation patterns for multi-component granular mixtures. In all presented simulations, there was a reasonable agreement (only qualitative for the last simulation) between experiments and simulations, and it is believed that the model constitutes a major advance over the current method for determining material segregation during core flow discharge of axisymmetric silo.

7. CONCLUSIONS

In this paper, a continuum mechanics framework, first introduced in Ref. [12], was implemented with micro-physical parametrizations to model particle segregation

during core flow discharge. The modified kinematic model of Nedderman [20] was employed for the computation of the stagnant zone boundaries and was appropriately extended for the modeling of cylindrical hoppers which incorporate conical sections (a type of hoppers commonly met in the process engineering industry). The model was then used to simulate discharges of multi-component mixtures from hoppers and study the effects of size segregation. The model was shown, through comparisons with available experimental data, to give a reasonable approximation of the behavior of granular mixtures.

The developed continuum framework, which employs micro-physical parametrizations for the description of segregation of granular mixtures in both mass and core flow processes, is believed to be unique. An important limitation of the present model is the determination of the initial conditions that have to be determined experimentally. Current work is focusing on the further validation of the model, so that ultimately it may constitute a powerful engineering tool which will assist in the optimization of existing industrial operations through reliable predictions of granular mixtures handling processes.

REFERENCES

1. A. W. Jenike, *Storage and Flow of Solids*, Utah Engineering Experimental Station Bulletin No. 123, University of Utah, Salt Lake City, UT (1964).
2. M. A. Goodman and S. C. Cowin, Two problems in the gravity flow of granular materials, *J. Fluid Mech.* **45**, 321–339 (1971).
3. C. Brennen and P. C. Pearce, Granular material flow in two-dimensional hoppers, *J. Appl. Mech.* **45**, 43–50 (1978).
4. C. S. Campbell and C. E. Brennen, Computer simulation of granular shear flows, *J. Fluid Mech.* **151**, 167–188 (1985).
5. P. Arteaga and U. Tüzün, Flow of binary mixtures of equal-density granules in hopper-size segregation, flowing density and discharge rates, *Chem. Eng. Sci.* **45**, 205–223 (1990).
6. P. A. Langston, U. Tüzün and D. M. Heyes, Discrete element simulation of internal stress and flow fields in funnel flow hoppers, *Powder Technol.* **85**, 153–169 (1995).
7. G. I. Tardos, A flow mechanistic approach to slow, frictional flow of powders, *Powder Technol.* **92**, 61–74 (1997).
8. T. Karlsson, M. Klisinski and K. Runneson, Finite element simulation of granular material flow in plane soils with complicated geometry, *Powder Technol.* **99**, 29–39 (1999).
9. S. A. Elaskar, L. A. Godoy, D. D. Gray and J. M. Stiles, A viscoplastic approach to model the flow of granular solids, *Int. J. Solids Struct.* **37**, 2185–2214 (2000).
10. P. W. Cleary and M. L. Sawley, DEM modelling of industrial granular flows: 3D case studies and the effect of particle shape on hopper discharge, *Appl. Math. Model.* **26**, 89–111 (2002).
11. P. C. Arnold, A. G. MacLean and A. W. Roberts, *Bulk Solids: Storage, Flow and Handling*, TUNRA Bulk Solids Handling Research Associates, University of Newcastle, NSW (1982).
12. N. Christakis, M. K. Patel, M. Cross, J. Baxter, H. Abou-Chakra and U. Tüzün, Predictions of segregation of granular material with the aid of PHYSICA, a 3-D unstructured finite-volume modelling framework, *Int. J. Numer. Meth. Fluids* **40**, 281–291 (2002).
13. A. W. Jenike, *Gravity Flow of Bulk Solids*, Utah Engineering Experimental Station Bulletin No. 108, University of Utah, Salt Lake City, UT (1961).

14. A. W. Jenike, A theory of flow of particulate solids in converging and diverging channels based on a conical yield function, *Powder Technol.* **50**, 229–236 (1987).
15. J. A. S. Cleaver and R. M. Nedderman, The measurement of velocity distributions in conical hoppers, *Chem. Eng. Sci.* **48**, 3703–3712 (1993).
16. J. Litwiniszyn, The model of a random walk of particles adapted to researches on problems of materials of loose materials, *Bull. L'Acad. Polon. Sci*. **11**, 61–70 (1963).
17. R. M. Nedderman and U. Tüzün, A kinematic model for the flow of granular materials, *Powder Technol.* **22**, 243–253 (1979).
18. U. Tüzün and R. M. Nedderman, Experimental evidence supporting kinematic modelling of the flow of granular media in the absence of air drag, *Powder Technol.* **24**, 257–266 (1979).
19. C. S. Chou, J. Y. Hsu and Y. D. Lau, The granular flow in a two-dimensional flat-bottomed hopper with eccentric discharge, *Physica A* **308**, 46–58 (2002).
20. R. M. Nedderman, The use of the kinematic model to predict the development of the stagnant zone boundary in the batch discharge of a bunker, *Chem. Eng. Sci.* **50**, 959–965 (1995).
21. G. R. Watson, Flow patterns in flat bottomed silos, PhD Thesis, University of Edinburgh (1993).
22. M. Cross, Computational issues in the modelling of materials based manufacturing processes, *J. Computer Aided Mater. Des.* **3**, 100–116 (1996).
23. J. Baxter, T. Gröger, U. Tüzün, H. Abou-Chakra, N. Christakis, M. K. Patel and M. Cross, Micro-mechanical parameterisations for continuum modelling of granular material using the discrete element method, in: *Proc. 5th World Congr. on Computational Mechanics (WCCM V)*, Vienna, http://wccm.tuwien.ac.at (2002).
24. K. A. Pericleous, G. J. Moran, S. Bounds, P. Chow and M. Cross, Three dimensional free surface flows modelling in an unstructured environments for metals processing applications, *Appl. Math. Model.* **22**, 895–906 (1998).
25. U. Tüzün, Velocity distributions in funnel flow bins, PhD Thesis, University of Cambridge (1979).
26. S. Masson and J. Martinez, Effect of particle mechanical properties on silo flow and stresses from distinct element simulations, *Powder Technol.* **109**, 164–178 (2000).
27. J. Crank, *Mathematics of Diffusion*, 2nd edn. Oxford University Press, London (1975).
28. O. C. Zienkiewicz and R. L. Taylor, *The Finite Element Method. Volume 2: Solid Mechanics*, 5th edn. Butterworh-Heinemann, London (2000).
29. H. Laux, Modelling of dilute and dense dispersed fluid-particle two phase flows, Dr. Ing. Thesis, The Norwegian University of Science and Technology (1997).
30. N. Christakis, P. Chapelle and M. K. Patel, Analysis and modeling of heaping behavior of granular mixtures within a computational mechanics framework, *Advanced Powder Technol.* **17**, 383–398 (2006).
31. G. F. Salter, Investigations into the segregation of heaps of particulate materials with particular reference to the effects of particle size, PhD Thesis, University of Greenwich (1999).
32. British Standards Institution, Test sieving: methods using test sieves of woven wire cloth and perforated metal plate, BS 1796: Part 1. BSI, London (1989).